ACS Infectious Diseases

pubs.acs.org/journal/aidcbc

Article

Plasmonic Fluor-Enhanced Antigen Arrays for High-Throughput, Serological Studies of SARS-CoV-2

Abraham J. Qavi,* Chao Wu, Matthew Lloyd, Mohammad Mahabub-Uz Zaman, Jingyi Luan, Claire Ballman, Daisy W. Leung, Scott L. Crick, Christopher W. Farnsworth,* and Gaya K. Amarasinghe*

Cite This: *ACS Infect. Dis.* 2022, 8, 1468−1479

Read Online

ACCESS | Metrics & More | Article Recommendations | Supporting Information

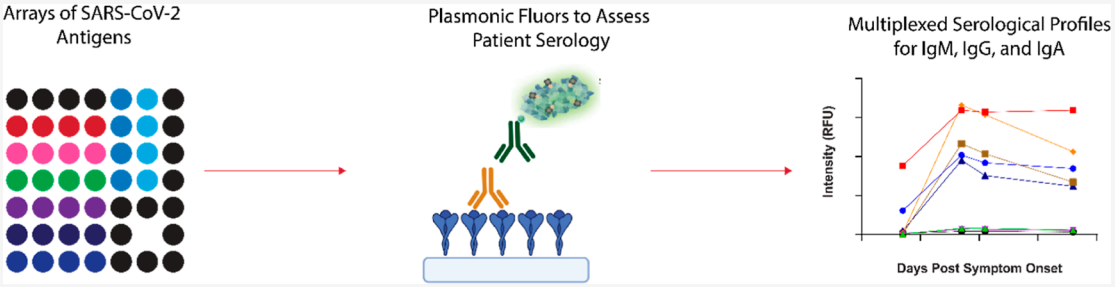

ABSTRACT: Serological testing for acute infection or prior exposure is critical for patient management and coordination of public health decisions during outbreaks. Current methods have several limitations, including variable performance, relatively low analytical and clinical sensitivity, and poor detection due to antigenic drift. Serological methods for SARS-CoV-2 detection for the ongoing COVID-19 pandemic suffer from several of these limitations and serves as a reminder of the critical need for new technologies. Here, we describe the use of ultrabright fluorescent reagents, Plasmonic Fluors, coupled with antigen arrays that address a subset of these limitations. We demonstrate its application using patient samples in SARS-CoV-2 serological assays. In our multiplexed assay, SARS-CoV-2 antigens were spotted into 48-plex arrays within a single well of a 96-well plate and used to evaluate remnant laboratory samples of SARS-CoV-2 positive patients. Signal-readout was performed with Auragent Bioscience's Empower microplate reader, and microarray analysis software. Sample volumes of 1 μL were used. High sensitivity of the Plasmonic Fluors combined with the array format enabled us to profile patient serological response to eight distinct SARS-CoV-2 antigens and evaluate responses to IgG, IgM, and IgA. Sensitivities for SARS-CoV-2 antigens during the symptomatic state ranged between 72.5 and 95.0%, specificity between 62.5 and 100%, and the resulting area under the curve values between 0.76 and 0.97. Together, these results highlight the increased sensitivity for low sample volumes and multiplex capability. These characteristics make Plasmonic Fluor-enhanced antigen arrays an attractive technology for serological studies for the COVID-19 pandemic and beyond.

KEYWORDS: *plasmonics, serology, screening, SARS-CoV-2, diagnostics*

Rapid screening for prior and active infection plays an important clinical role for assessing seroprevalence, evaluating the immune status of previously infected or vaccinated patients, and for diagnosis.[1−4] The ongoing SARS-CoV-2 pandemic has further magnified the deficiencies of current analytic and diagnostic assays. For example, commercially available serologic assays have high variable performance as a result of assay design with results dependent on the time from infection, an individual's immune responses, collection of the samples, the target antigen of the assay, and the antibody class targeted.[5−14]

There are two major classes of serological assays that have been employed for the detection of SARS-CoV-2 infections: lateral flow assays (LFAs) and enzyme-linked immunosorbent assay (ELISA)-based assays. LFAs offer the advantage of portability, ease of use, and rapid time-to-result, often under 30 min.[15] However, the trade-off with these devices is a lack of quantitative readout (e.g., titers), a limited ability to multiplex measurements, and a decrease in analytical sensitivity and specificity relative to more traditional laboratory-based methods.[16,17] There is also an enormous amount of variation in LFA-based testing.[16,18−20] ELISAs offer high-throughput screening capabilities that are quantitative but often require a centralized laboratory to perform the testing in addition to a

Received: February 10, 2022
Published: July 22, 2022

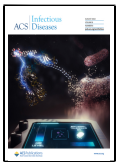

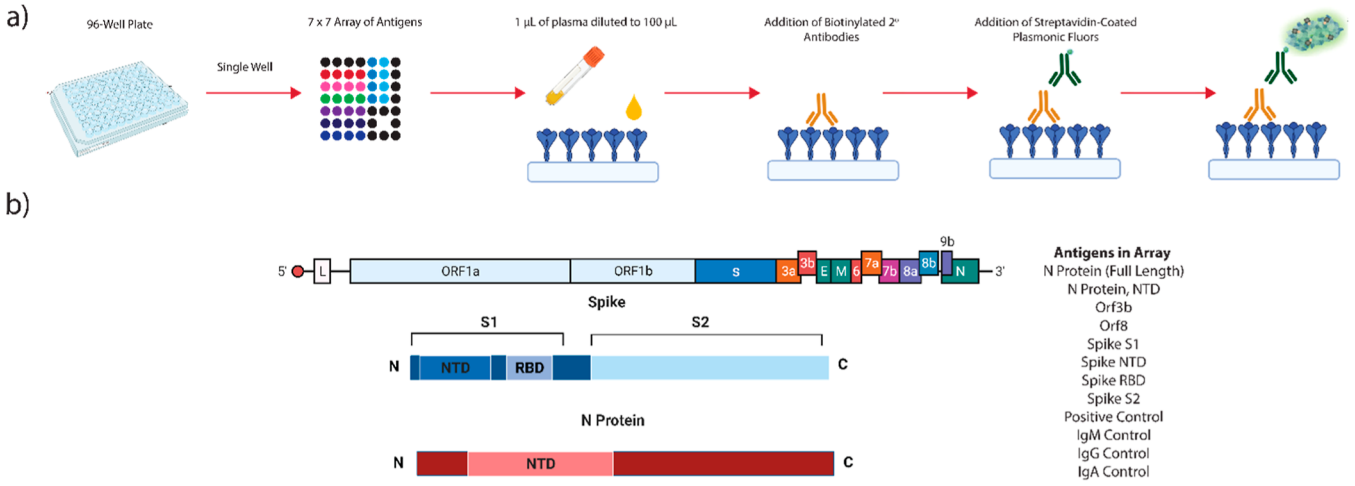

Figure 1. Workflow for assessing patient serology using arrays of SARS-CoV-2 antigens with Plasmonic Fluors and antigens utilized in arrays. (a) Within a single well of a 96-well plate, four individual antigen spots and one blank are arrayed in a 7 × 7 format. A diluted human serum sample is added to each well, after which, biotinylated secondary antibodies against human IgM, IgG, and IgA are incubated with the array. Streptavidin-coated Plasmonic Fluors are added to each well, and serological response assessed. (b) Genome of SARS-CoV-2, with magnification of the N and spike proteins. Protein arrays consisted of N FL, N NTD, Orf3b, Orf8, spike S1, spike NTD, spike RBD, spike S2, and control spots (figure created with Biorender.com).

a)

PC	PC	PC	PC	SPIKE RBD	SPIKE S2	IgG
N FL	N FL	N FL	N FL	SPIKE RBD	SPIKE S2	IgG
N NTD	N NTD	N NTD	N NTD	SPIKE RBD	SPIKE S2	IgG
Orf3b	Orf3b	Orf3b	Orf3b	SPIKE RBD	SPIKE S2	IgG
Orf8	Orf8	Orf8	Orf8	IgM	IgM	IgM
SPIKE S1	SPIKE S1	SPIKE S1	SPIKE S1	IgM	EMPTY	IgA
SPIKE NTD	SPIKE NTD	SPIKE NTD	SPIKE NTD	IgA	IgA	IgA

b)

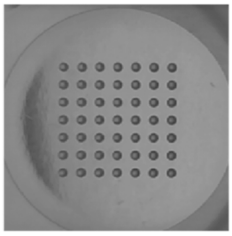

c)

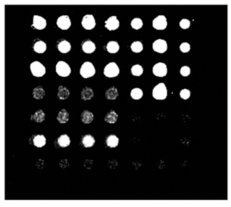

Figure 2. Antigen identities within each spot of the microarray and printed arrays. (a) Array alignment and orientation of antigens. PC = positive control. IgM, IgG, and IgA refer to positive control spots for human IgM, IgG, and IgA respectively. A single spot was left empty for alignment purposes. (b) Optical micrograph of a 7 × 7 array of spotted antigens. (c) Fluorescent readout of an array following exposure to human plasma, secondary antibodies, and Plasmonic Fluors.

longer assay time (>60 min as compared to 15 min for LFAs). While multiplexing capabilities are possible, this either comes at a cost of sensitivity or additional sample volume.

Plasmonic Fluors are ultrabright fluorescent nanocomposites with a brightness many thousands of times that of traditional organic fluorophores.[21−24] The fundamental principle behind Plasmonic Fluors is plasmon-enhanced fluorescence.[25] It is well established that metallic nanostructures, often consisting of gold and silver, can support localized surface plasmon resonance (LSPR),[26,27] which results in a focal enhancement of electromagnetic fields. This field enhancement has been used in the context of a variety of sensing applications, including surface plasmon resonance imaging (SPRI),[28] surface-enhanced Raman spectroscopy (SERS),[28−30] and a variety of optical antennae.[31−34] Precise control of the LSPR emission wavelength, lifetime, and intensity can be tuned by varying the geometry and aspect ratio of the nanostructures.[35] The ability to tune their optical properties enable their coupling to fluorescence molecules, thereby drastically improving the fluorescence intensity and efficiency. In the context of Plasmonic Fluors, precise optimization of the distance between the nanoparticles and fluorophores has enabled a means to maximize fluorescence while minimizing non-radiative energy transfer.[21] When employed as a reporter molecule in immunoassays, this improved fluorescence efficiency results in an improved analytical limit of detections, the ability to use smaller sample volumes, and more rapid readout times.[21−24]

Here, we demonstrate the use of Plasmonic Fluors as a reporter molecule in combination with arrays of SARS-CoV-2 antigens and assay readout using an Auragent Bioscience's low-cost Empower microplate reader as a proof of concept to demonstrate the utility of high throughput, multiplexed,

https://doi.org/10.1021/acsinfecdis.2c00086
ACS Infect. Dis. 2022, 8, 1468−1479

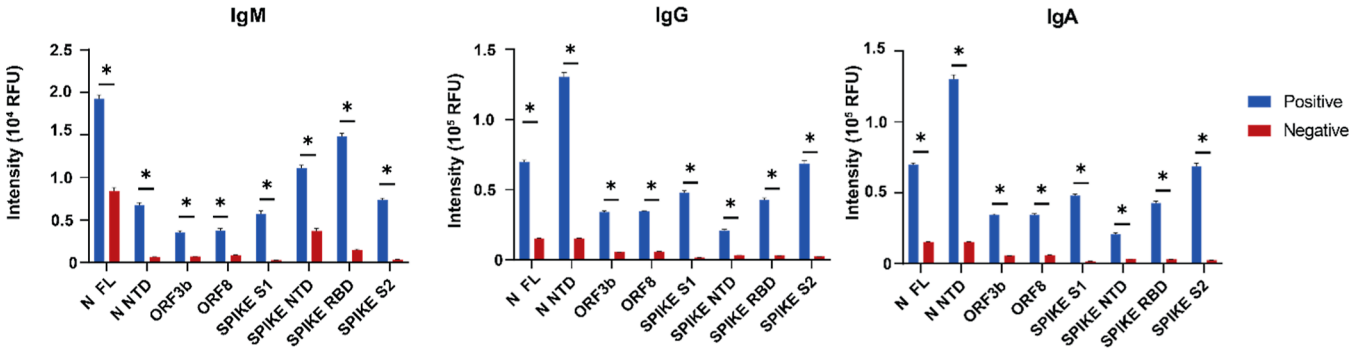

Figure 3. Serological responses for each antigen and immunoglobulin combination from SARS-CoV-2 positive and negative patients. Average serological response for each antigen in SARS-CoV-2 positive (blue) and negative (red) patients, for (a) IgM, (b) IgG, and (c) IgA. Error bars represent the standard error of the mean (SEM) for four technical replicates. * denotes a p-value of $<1 \times 10^{-6}$.

ultrasensitive serological assays. The high sensitivity enabled by the Plasmonic Fluors (up to 10^3 improvement over conventional ELISAs[21]) combined with the array format enabled us to profile patient serological response to eight separate SARS-CoV-2 antigens for IgG, IgM, and IgA. We were able to establish sensitivity and specificity cutoffs for each of these markers, for a total of 24 combinations using sample volumes as low as 1 μL of patient plasma. We also show the evolution of serological response for each antigen as a function of time since symptom onset with the potential for clinically actionable decisions. Together, these results highlight the potential impact of Plasmonic Fluors as a reporter for infections and a flexible tool to address rapidly evolving public health crises.

RESULTS

The key features of the overall experimental platform, including the workflow schematic of experiments with the Plasmonic Fluors are shown in Figure 1. Briefly, in a single-well of a 96-well plate, a 7 × 7 array of both antigens of interest and controls are deposited with a microarray spotter. Human plasma diluted 1:100 to a total volume of 100 μL is incubated in the wells, after which a biotinylated anti-human IgG, IgM, or IgA antibody is added to the wells. A streptavidin-conjugated Plasmonic Fluor is subsequently added to the wells, after which the fluorescent signal is read using the Auragent Bioscience's Empower plate reader. Fluorescent intensities were automatically calculated using Auragent Bioscience's microarray analysis software.

To construct arrays for SARS-CoV-2 serology, we initially spotted 7 × 7 arrays of antigens and controls. Figure 2a highlights the antigen spotting pattern within a single well of a 96-well plate. Eight antigens of interest were spotted in quadruplicate. Each array also contained a positive control of biotinylated IgG, as well as IgM, IgG, and IgA specific controls, all also spotted in quadruplicate. The positive controls for IgM, IgG, and IgA were validated with spike-in studies in neat, buffered solutions and are highlighted in Figure S1. Cross-reactivity between the secondary antibodies for IgM, IgG, and IgA was also assessed, with minimal cross-reactivity between off-target pairs (Figure S2). The antigens used in our assay were chosen based on previous literature reports[36,37] as well as availability both within our laboratory and commercial sources. A blank spot was included for alignment purposes in automated analysis. An optical image of the array is shown in Figure 2b, with a representative fluorescent readout in Figure 2c.

Figure 3 and Table S1 highlight the average serological response for each antigen assessed in our assay, for both SARS-CoV-2 positive (n = 20 patients, four samples for each patient resulting in 80 samples) and negative patients (n = 16 patients, one sample for each patient resulting in 16 samples). There was a statistically significant difference between the intensities of the positive and negative patients for each of the 24 antigen−immunoglobulin combinations. For IgG response, N_{NTD} had the highest response, followed by N FL and spike S2. For IgM, N FL had the highest response, followed by spike RBD and spike NTD. For IgA, the highest intensity signal was N_{NTD}, followed by N FL, and spike S2. Except for spike RBD, the average intensity of the IgM response for every antigen was lower than that for IgG and IgA. IgG and IgA responses varied in terms of which had a higher signal. For example, the IgG responses toward N FL and N NTD were higher than the IgA response, but the converse was true with Orf3b and Orf8. The average response among the negative patients for each antigen has less variability than positive patients, as expected.

Using these values, we generated receiver−operator characteristic (ROC) curves for each of the antigens and immunoglobulins (Figure S3) and established cutoffs via Youden's index (J).[38] From these values, we determined the sensitivity and specificity of each marker individually, as highlighted in Table 1. Of note, these metrics were determined for all positive patient samples, with days post-symptom infection ranging from 0 to 60 days (average = 21.4 days, median = 20 days). For IgG, the sensitivity ranged from 85.00 to 98.75%, while the specificity ranged from 64.71 to 100%. For IgM, sensitivity ranged from 72.50 to 92.50%, and specificity ranged from 62.50 to 100%. For IgA, sensitivity ranged from 85.00 to 95.00%, and specificity ranged from 87.50 to 100%.

Serological response for each marker as a function of time, from 0 to 60 days post-symptom onset, are highlighted in Figure 4. Antigens had variability in terms of a positive or negative correlation over time between IgM, IgG, and IgA. For example, N NTD had a positive correlation over time for IgM and IgA but a negative correlation for IgG. In contrast, spike S1 had a positive correlation for IgM, IgG, and IgA (Figure S4 and Table S2). Furthermore, there was a measurable response that was higher than the established cutoffs as early as 0 days post-symptom onset for each of the antigen−immunoglobin combinations assessed in our studies.

Next, we evaluated the serological response from two representative patients (patients #15 and #20, Table S3) over

https://doi.org/10.1021/acsinfecdis.2c00086
ACS Infect. Dis. 2022, 8, 1468−1479

Table 1. Assay Performance Characteristics[a]

antigen	sensitivity	specificity	AUC	intensity cutoff(RFU)
		IgM		
N FL	72.50	68.75	0.77	6989
N NTD	92.50	78.57	0.92	681
Orf3b	85.00	81.25	0.90	1000
Orf8	72.50	93.75	0.90	1410
spike S1	73.75	100.00	0.89	588
spike NTD	81.25	62.50	0.76	2382
spike RBD	83.75	93.75	0.93	2499
spike S2	75.00	100.00	0.92	883
		IgG		
N FL	92.50	88.24	0.92	8507
N NTD	87.50	100.00	0.96	5372
Orf3b	98.75	64.71	0.85	1606
Orf8	85.00	82.35	0.85	5886
spike S1	85.00	94.12	0.94	1875
spike NTD	87.50	88.24	0.89	3165
spike RBD	86.25	100.00	0.97	2521
spike S2	87.50	100.00	0.96	3838
		IgA		
N FL	91.25	93.75	0.90	18,256
N NTD	91.25	93.75	0.90	14,736
Orf3b	85.00	100.00	0.94	15,550
Orf8	93.75	87.50	0.94	10,495
spike S1	92.50	100.00	0.95	5284
spike NTD	90.00	100.00	0.94	7478
spike RBD	95.00	100.00	0.95	7306
spike S2	93.75	100.00	0.96	7218

[a]Sensitivity, specificity, and area under the curve (AUC) determined from ROC curves for each serological marker assessed in our study.

the course of their SARS-CoV-2 infection (Figure 5). For both patients, the IgG response reaches a maximum around 20 days. However, for patient #20 (Figure 5a), the IgG response remained relatively constant, whereas in patient #15, this response declined with time (Figure 5d). The IgM response for both patients decreased over the time-course for N FL and spike NTD and increased for spike S1 and spike RBD with a maximum around 20 days. Finally, the IgA response for both patients peaked around 20 days, followed by a decline in the signal for most of the antigens. The serological response for all 20 patients over the course of their SARS-CoV-2 infection can be found in Supporting Information (Figure S5). There is variability in the serological response for each patient examined in the study.

To demonstrate the ability to further multiplex serological measurements, we sought to detect IgM, IgG, and IgA responses from a single well instead of three separate wells. Figure 6 highlights hand-spotted 2 × 2 arrays in each well consisting of spike S1-RBD, spike S2, N FL, and a control containing a mixture of human IgG, IgM, and IgA, and readout using three spectrally distinct Plasmonic Fluors (PF_{800}, PF_{650}, and PF_{550}) which are spectrally similar to Licor's IR Dye 800CW, Cy5, and Cy3, respectively. To perform these experiments, streptavidin-conjugated Plasmonic Fluors were first coated with biotinylated IgM (PF_{650}), IgG (PF_{800}), and IgA (PF_{550}). All three combinations were added simultaneously, and the wells were imaged using an Azure Sapphire laser scanner system. As demonstrated in Figure 6 (Figure S6 and Table S5), it was possible to resolve the individual fluorophores corresponding to the IgG, IgM, and IgA serological response, in a single well, from a single sample, over multiple patient samples.

DISCUSSION

In this study, we demonstrate the potential clinical utility of a novel, multiplexed, high sensitivity Plasmonic Fluor to simultaneously assess the serological response to eight separate SARS-CoV-2 antigens, for IgG, IgM, and IgA. Importantly, the serological profiles highlighted in our study are consistent with previously reported reports; maturation of serological response typically follows a classical viral pattern; initially IgM, followed closely by IgA, and finally IgG (Figure 4).[39,40] There are instances in which there were deviations from this, such as detection of IgM and IgA simultaneously,[41] IgG seroconversion before IgM,[39] and simultaneous IgM and IgM, although these appear to be the exception,[42] and it is unclear whether these differences reflect underlying differences in the serological assays or patient responses. Interestingly, we also observed different dynamics of the serological response to different antigens in each patient. The clinical relevance of this finding requires a follow-up study.

Another interesting finding was the sensitivity and specificity of IgA among the immunoglobulins tended to be higher than IgM and IgG (although not for all antigens). This is consistent with previous literature reports, indicating an increase in IgA early in the course of SARS-CoV-2 infection.[43] The reason for the increased analytical performance of IgA thus may reflect design of the assay or a biological basis within the patient population we studied.

An advantage of the technique presented here is the adaptability with different antigens. Most commercially available serological assays for SARS-CoV-2 infection rely on the N or S antigens as markers for infection. Previous reports in the literature, including our own work, have demonstrated that use of other SARS-CoV-2 antigens for serological response, as well as using specific protein truncations, can improve the analytical performance of assays.[36,37] Hachim et al. demonstrated that by combining the serological response of SARS-CoV-2 Orf3b and Orf8, analytical performance of their assay improved to 96.5% sensitivity and 99.5% specificity. Furthermore, our previous work demonstrated that truncations of the SARS-CoV-2 N protein elicited differential serological responses. The ability to use multiple antigens in addition to protein truncations can improve the analytical performance and flexibility of the assay design.[37] Additionally, there is concern of cross-reactivity due to the prior infection with seasonal coronaviruses. Seasonal coronaviruses, namely 229E, HKU1, NL63, and OC43, have a prevalence as high as 90% in the adult population.[44] Several studies have demonstrated cross-reactivity between the SARS-CoV-2 S protein with other coronavirus N protein.[45−48] A study by Anderson and colleagues found that 4.2% of serum samples collected pre-pandemic in 2017 had IgG antibodies reactive against SARS-CoV-2 full-length spike, 0.93% of samples reacted toward SARS-CoV-2 spike RBD, and 16.2% were reactive to SARS-CoV-2 N protein.[47] Because of the flexible design of our arrays, we can rapidly substitute antigens of interest into the assay design to optimize the performance. While further studies are needed, this technology also is adaptable to SARS-CoV-2 variants, allowing for the rapid assessment of the serological response to several strains simultaneously.

One interesting result of our study was the number of patients with a detectable serological response less than 7 days

https://doi.org/10.1021/acsinfecdis.2c00086
ACS Infect. Dis. 2022, 8, 1468−1479

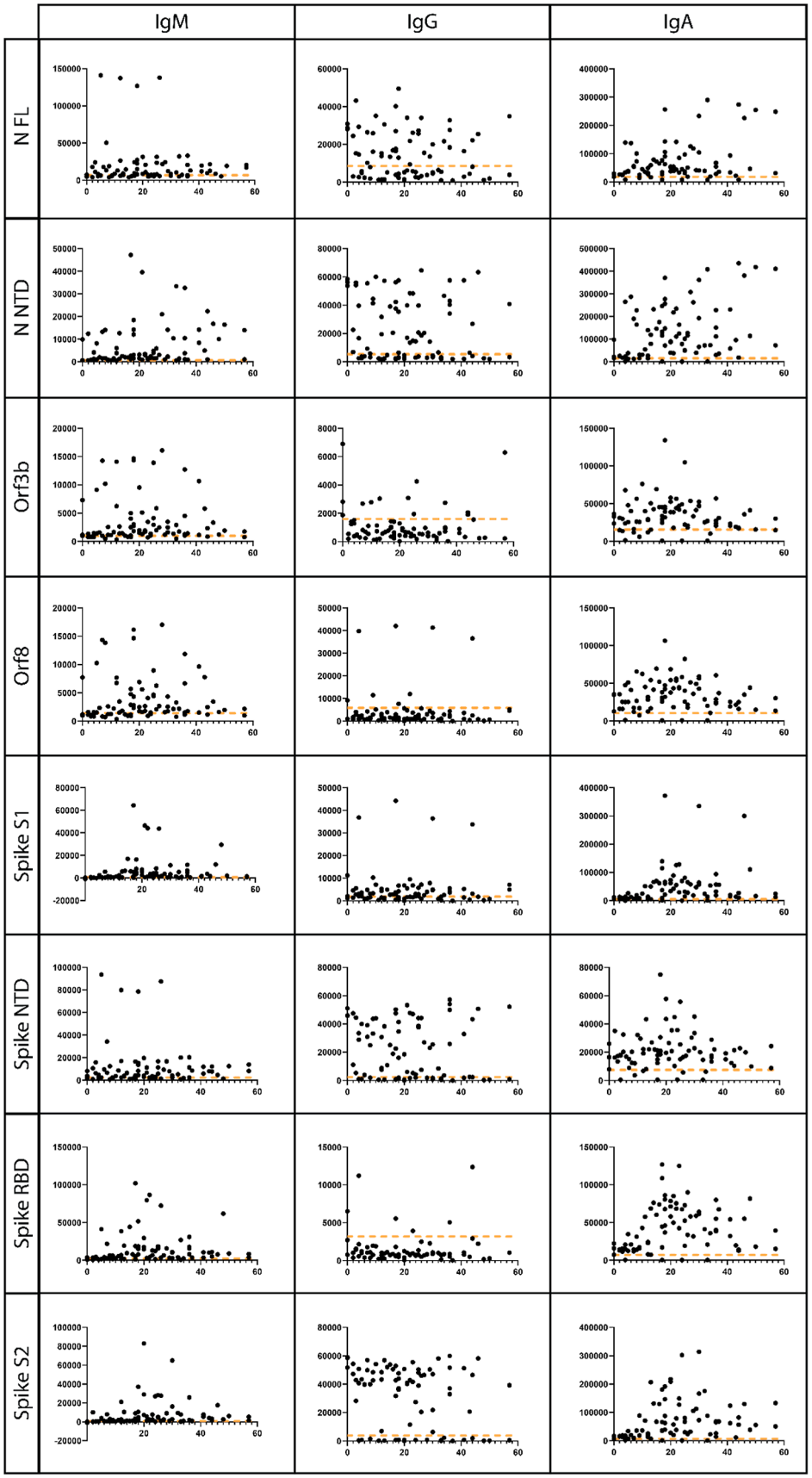

Figure 4. Serological responses for each antigen as a function of time. Vertical columns represent the IgM, IgG, and IgA (left to right) responses for each antigen for 80 separate, positive samples from 0 to 60 days post-symptom onset. Each horizontal row represents a specific SARS-CoV-2 antigen. The orange dashed line represents the cutoff value used in determining the sensitivity and specificity calculations in Table 1. The *y*-axis for each graph shows the intensity (RFU), and the *x*-axis days shows the post-symptom onset, ranging from 0 to 60.

https://doi.org/10.1021/acsinfecdis.2c00086
ACS Infect. Dis. 2022, 8, 1468−1479

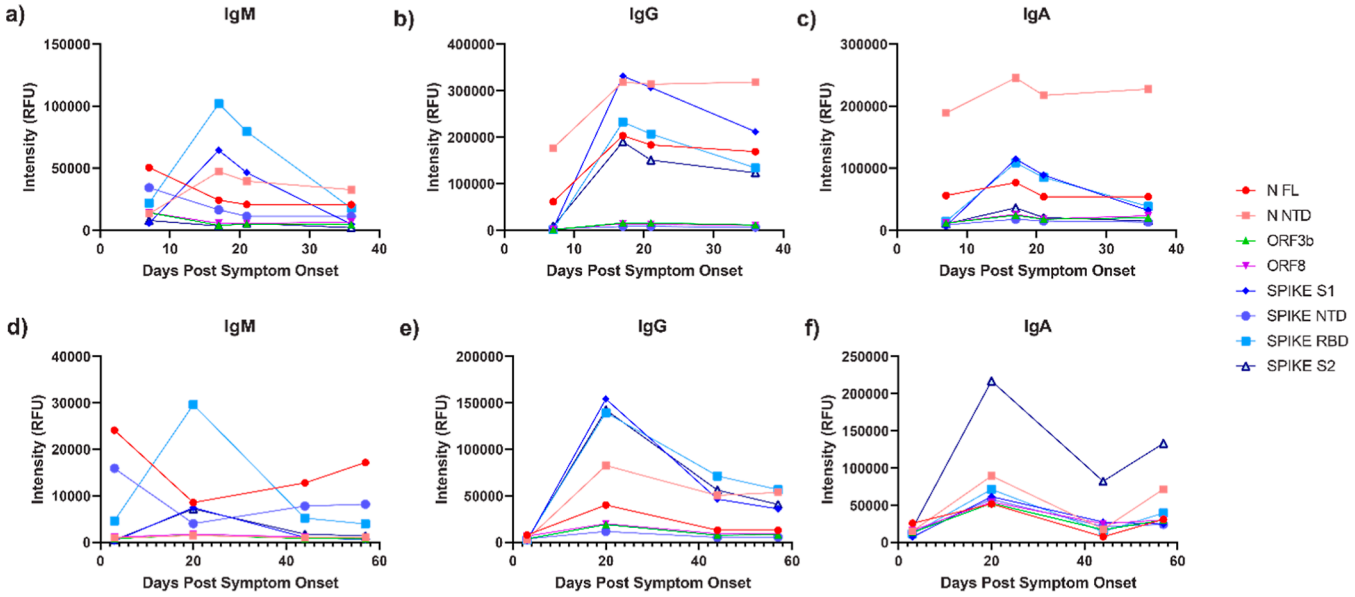

Figure 5. Serological response for eight SARS-CoV-2 antigens for patients longitudinally. Serological response to eight separate antigens for IgM (a,d), IgG (b,e), and IgA (c,f) were assessed throughout a hospital stay. (a−c) represent a single patient (patient #20), whereas (d−f) represent another patient (patient #15).

from the symptom onset. Previous literature reports have reported the median seroconversion time between 12 and 15 days post-symptom onset for IgG, 4−14 days for IgM, and 4−24 days for IgA.[49] Our ability to detect infection early in the disease process reflects a combination of the following: (1) increased analytical sensitivity of our assay, enabling us to detect serological responses that other assays miss, (2) cross-reactivity of the antigens due to the prior infection with other coronaviruses, and (3) inconsistencies in reporting days post-symptom onset. Nonetheless, it is tempting to speculate that the early detection of antibodies to SARS-CoV-2 was a result of the Plasmonic Fluor technology coupled with a multiplexed assay design targeting multiple epitopes. Previous work with Abbott SARS-CoV-2 serological assay demonstrated a sensitivity of 30.0% for specimen with the symptom onset up to 7 days.[14] In comparison, the sensitivity for IgM, IgG, and IgA from samples up to 7 days following symptom onset with our assay for N FL was 73.33, 88.24, and 93.33% respectively.

This study also demonstrates the use of Plasmonic Fluors in an array format, as a facile pipeline for serological studies. The ability to substitute antigens of interest, assess IgM, IgG, and IgA levels, and screen patient samples with as little as 1 μL of patient plasma enable this technology as a powerful tool. Many commercial laboratory analyzer systems used in clinical laboratories leave a dead volume of 100 μL, or greater; thus, our technique is well situated to use remnant patient samples.[50] While many current ELISAs use a relatively low volume of patient plasma (e.g., 100 μL/well[51]), the combination of multiplex measurements and high sensitivity (further reducing volume requirements) allows us to perform our analysis in a single well, with only 1 μL of plasma. Dried blood spot ELISAs (DBS−ELISAs)[52,53] offer an alternative to the high-volume requirements seen with many conventional ELISAs. In this technique, dried spots of blood are stored on a nitrocellulose paper, until they can be reprocessed and analyzed via ELISA. Brinc and colleagues demonstrated that while antibody levels for SARS-CoV-2 spike protein were reduced following use of DBS, there was high correlation with the commercial assays.[54] This technique, however, does not overcome the sensitivity or multiplexed challenges faced by conventional ELISAs.

Given the low-volume requirements, we can also incorporate this testing into routine laboratory testing of patients, without the need for additional patient draws, reducing the risk of iatrogenic anemia.[55−57] The ability to survey patients longitudinally throughout their SARS-CoV-2 infection can now easily be run concurrently with the prior laboratory workflow. Longitudinal assessment will provide healthcare workers with quantitative trends in serology versus the current, absolute values for assay (positive/negative) that were obtained on a population. Given the significant number of variables in serological response in patients (e.g., patient age, immune status, and co-morbidities), monitoring trends in serology offer a more in-depth snapshot of a patient's infection.

The combination of multiplexed measurements within a single well, the ability to interrogate IgM, IgG, and IgA together, and the flexibility of the assay format are key advantages of our technique. We have provided a comparison of our assay with existing SARS-CoV-2 serological assays, as listed in Table S6. Of note, the reported sensitivity and specificity of each assay depend on several factors, including the instrument gain, incubation times, assay design, and patient samples utilized. Previous studies have highlighted that hospitalized patients have different serological responses than non-hospitalized patients.[58,59] Therefore, it is difficult to compare the analytical performance of the assays in a meaningful way. In contrast, we have highlighted characteristics of serological assays that may influence researchers and healthcare providers in their decision-making.

During the course of submission of this article, Wang et al. published a study leveraging Plasmonic Fluors for the detection of SARS-CoV-2 serology via linear epitopes of the spike protein.[60] This work reinforces the practical utility of Plasmonic Fluors in serological studies, in addition to their improved sensitivity over traditional fluorescence probes. While the study demonstrated an improvement in sensitivity

https://doi.org/10.1021/acsinfecdis.2c00086
ACS Infect. Dis. 2022, 8, 1468−1479

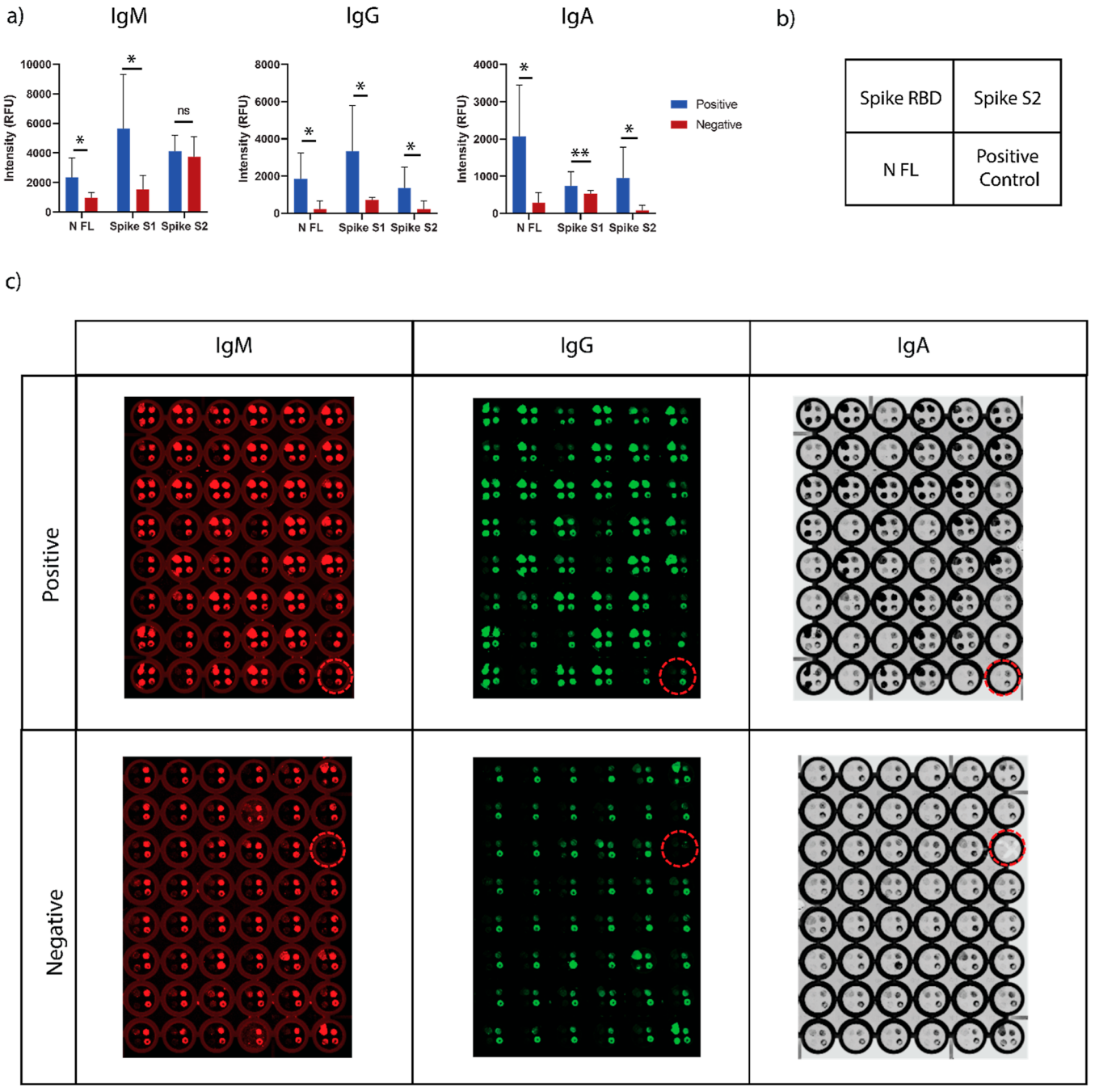

Figure 6. Multiplexed detection of immunoglobulins in a single well and sample. (a) Simultaneous detection of IgM, IgG, and IgA serological response in a single, hand-spotted well containing spike RBD, spike S2, N FL, and a control. * denotes $p < 1 \times 10^{-6}$, ** denotes $p < 0.001$, and ns denotes no statistical significance. (b) Array alignment and orientation of antigens. (c) False-color images obtained from a single 96-well plate for both positive and negative patient cohorts corresponding to (a). The dashed circles highlight wells omitted from analysis.

of ~100-fold over conventional ELISAs in addition to a 20 min assay time, there was limited multiplexing (e.g., 2 targets) performed in this format. Our study has a number of key differences from this work, including significantly increased multiplexing capabilities, the detection of IgM, IgG, and IgA, and longitudinal studies of patient serological responses. Our assay design enables a much more streamlined and flexible approach toward serological studies that can be adapted toward a variety of pathogens.

While our study addresses many key limitations in the field, there are several limitations with the present study, which we are actively working to address. For example, days post-symptom onset for each of the patient samples relied on physician encounter notes and were often patient reported. Given the asymptomatic window of many patients present with SARS-CoV-2, this can be problematic in determining the actual onset of infection.[38] Patient reporting of symptoms is also problematic, in that many patients will under report or not recognize early symptoms of respiratory infections.[61] Furthermore, positive patients in this study were hospitalized at a tertiary, academic medical center as a result of COVID-19 symptoms and thus represent more severe cases. It is well established that patients with more severe SARS-CoV-2 infections have a more rapid and significant serological

https://doi.org/10.1021/acsinfecdis.2c00086
ACS Infect. Dis. 2022, 8, 1468−1479

response.[62−64] This likely skewed our data toward patients with more severe infections and higher serological responses. We anticipate that with less severe or asymptomatic patients, the signal will be lower, however, that we can also use additional patient plasma to account for this difference.

An analytical consideration moving forward is multiplexing the readout in a single well. While we can use Plasmonic Fluors with different fluorescent emissions, further optimization is needed before we can quantitatively determine IgM, IgG, and IgA response from a single well. Due to the size of the array spots, as well as limited binding sites for each antigen, there is concern of competition of the secondary antibodies used in our assay.

METHODS

Plasmonic Fluors. Plasmonic Fluors were obtained from Auragent Bioscience. Unless otherwise specified, all microarrays were probed with streptavidin-conjugated PF_{650} which has excitation and emission spectra similar to Cy5.

Proteins. Biotinylated Anti-Human IgM μ-Chain-Specific, Anti-Human IgG Fc Specific, and Goat Anti-Human Serum IgA Alpha Chain-Specific were all obtained from Leinco. Recombinant SARS-CoV-2 full length nucleocapsid (N) protein and recombinant SARS-CoV-2 spike RBD protein were also obtained from Leinco. Recombinant SARS-CoV-2 spike S1 protein was obtained from Sino Biological, and recombinant SARS-CoV-2 spike S2 protein was obtained from Biovision. Recombinant ORF3b, ORF8, and SARS-CoV-2 N NTD proteins were generated, as previously described.[37]

Array Spotting. Antigens were spotted using a NanoPlotter (GeSiM). Each antigen or control spot was printed onto a Greiner Bio-One plate (model 655097) at a concentration of 10 μg/mL in printing buffer consisting of 10% glycerol in PBS. A schematic and optical micrograph of each individual array within a well is shown in Figure 2. Each well contained a 7 × 7 array of spots, with individual identities of each spot shown in Figure 2a. In addition to assessing antigens of interest, each array additionally had positive controls of biotinylated IgG and controls for human IgM, IgG, and IgA (n = 4 of each) to assess whether the assay was performing as expected. There was also a single spot left blank in the array for alignment purposes. After printing, the plate was blocked with 200 μL of 3% BSA with 0.05% Tween-20 for 30 min and subsequently rinsed with PBST three times prior to use.

Assay Performance—Single Fluor within a Well. 1 μL of patient plasma was diluted 100× using 3% BSA + 0.2% TritonX100. 1 μL of sample was used as our standard volume since it provided the largest flexibility given our instrumentation. It provided good discrimination between positive and negative patient samples, without saturation of the signal, and with a dynamic range that suited our needs. 100 μL of the 100× diluted plasma was added into each well and incubated for 1 h. The wells were washed three times with PBST. 100 μL of biotinylated anti-IgG (50 ng/mL) or 100 μL of biotinylated-Anti-IgM (50 ng/mL) or 100 μL of biotinylated-Anti-IgA (10 ng/mL) in 3% BSA was added into the respective wells and incubated for 1 h at room temperature. Wells were washed three times with PBST, followed by the addition of 75 μL of streptavidin-conjugated PF_{650} in 3% BSA for 20 min at room temperature. Finally, the wells were rinsed five times with PBST and readout with the Auragent Bioscience's Empower reader, a single-wavelength plate reader optimized for reading microarrays probed with PF_{650}. The fluorescent intensity of each individual spot in the array was automatically determined using Auragent Bioscience's array analysis software. Each antigen or control consisted of four technical replicates.

Specificity of IgM, IgG, and IgA Secondary Antibodies. Hand-spotted antigens (IgM, IgG, and IgA) were spotted at a concentration of 1 μg/mL of N protein in quadruplicate into each well of a 96-well plate. The spots were left in the plate at 37 °C for 2 h to dry. The plate was blocked with a solution of 3% BSA in PBST for 1 h. The plate was washed three times with PBS, after which PF800CW-anti-IgA, PF800CW-anti-IgG, and PF800CW-anti-IgM were added to their respective rows and incubated for 1 h. The plates were rinsed four times with PBST prior to readout with a Sapphire Biomolecular Imager.

Antigens in the 7 × 7 array were spotted, as described above, with the exception of the antigens being spotted at a concentration of 5 μg/mL. After printing, the plate was blocked with 200 μL of 3% BSA with 0.05% Tween-20 for 30 min. The plate was rinsed with 200 μL of PBST three times. Afterward, 100 μL of 3% BSA + 0.2% TritonX100 was added into each well and incubated for 1 h—this was in lieu of a patient sample. The plate was washed with 200 μL of PBST three times. 100 μL of biotinylated-anti-IgG (50 ng/mL), biotinylated-anti-IgM (50 ng/mL), or biotinylated anti-IgA (10 ng/mL) in 3% BSA was added into each well and incubated for 1 h. The wells were washed three times with 200 μL of PBS. Next, 75 μL of PF_{650} in 3% BSA was added to each well for 20 min. The wells were washed five times with 200 μL of PBST, prior to readout with the Auragent Bioscience's Empower reader.

Assay Performance—Multiplexed Fluors within a Well. Dilution of patient plasma in addition to assay steps were identical to that previously described for a single fluor within a well. For multiplexed readout, three separate Plasmonic Fluors for each anti-human Ig were utilized—PF_{800} with anti-IgG, PF_{650} with anti-IgM, and PF_{550} with anti-IgA. The images were acquired simultaneously on a Sapphire Biomolecular Imager (Azure Biosystems) using three predefined channels (Cy3, Cy5, and 800CW). Intensities for each of the channels were set as follows: Cy3 (intensity 5), Cy5 (intensity 3), and 800CW (intensity 1). The scan speed was set to "highest," focus position to "plate," and pixel size to "100 μm." The data (Table S5) represent the mean intensity of each spot, as determined by hand using the Azure analysis toolbox. For positive samples, a single sample was excluded due to a lack of positive control appearing in any channel. For negative samples, a sample was excluded due to the manual error. Following these exclusions, there was a total of 47 positive patients (each with 1 sample, for a total of 47 samples) and 47 negative patients (each with 1 sample, for a total of 47 samples).

Software and Statistical Analyses. Generation of ROC curves and AUC were carried out in GraphPad Prism 9. A Student's t test was used to determine significance between positive and negative serological responses. Images were generated using GraphPad Prism 9 and Adobe illustrator.

Samples. Patient samples were obtained from Barnes-Jewish Hospital (St. Louis, MO, USA), an academic, tertiary medical center. Samples were collected following the start of the pandemic from symptomatic patients with RT-PCR confirmed SARS-CoV-2 infection, or for negative controls, RT-PCR and symptomatic confirmed negative. Remnant

https://doi.org/10.1021/acsinfecdis.2c00086
ACS Infect. Dis. 2022, 8, 1468−1479

clinical samples were collected in the lavender top, EDTA BD vacutainer tubes for physician ordered complete blood count. Samples were stored for <2 days at 4 °C, centrifuged at 3500 rpm for 10 min, and the plasma stored at −80 °C until analysis. Collection was approved by the Human Research Protection Office at Washington University in St. Louis, Institutional Review Board Reference Number 202007097. Tables S3 and S4 highlight the patient demographics of samples utilized in this study. Time from the symptom onset was adjudicated by two independent physicians using physician encounter notes from the electronic medical record (EPIC).

■ ASSOCIATED CONTENT

Supporting Information

The Supporting Information is available free of charge at https://pubs.acs.org/doi/10.1021/acsinfecdis.2c00086.

Specificity of biotinylated-secondary antibodies, cross-reactivity of secondary antibodies, receiver−operator curves for antigen−immunoglobulin responses, serological response for the multiplexed assay with 20 patients, multiplexed detection of immunoglobulins in a single well from a single sample, cross-reactivity between commercial fluors in a single-well multiplxed measurement, patient demographics from the study, and intensity readouts for each antigen combination (PDF)

■ AUTHOR INFORMATION

Corresponding Authors

Abraham J. Qavi − *Department of Pathology & Immunology, Washington University School of Medicine, St. Louis, Missouri 63110, United States*; Email: abrahamqavi@wustl.edu

Christopher W. Farnsworth − *Department of Pathology & Immunology, Washington University School of Medicine, St. Louis, Missouri 63110, United States*; Phone: 314-362-1503; Email: cwfarnsworth@wustl.edu

Gaya K. Amarasinghe − *Department of Pathology & Immunology, Washington University School of Medicine, St. Louis, Missouri 63110, United States*; orcid.org/0000-0002-0418-9707; Phone: 314-286-0619; Email: gamarsasinghe@wustl.edu

Authors

Chao Wu − *Department of Pathology & Immunology, Washington University School of Medicine, St. Louis, Missouri 63110, United States*

Matthew Lloyd − *Department of Pathology & Immunology, Washington University School of Medicine, St. Louis, Missouri 63110, United States*

Mohammad Mahabub-Uz Zaman − *Auragent Bioscience, St. Louis, Missouri 63108, United States*

Jingyi Luan − *Auragent Bioscience, St. Louis, Missouri 63108, United States*; Present Address: Wyss Institute for Biologically Inspired Engineering, Harvard University, Boston, MA, 02115, United States

Claire Ballman − *Department of Pathology & Immunology, Washington University School of Medicine, St. Louis, Missouri 63110, United States*

Daisy W. Leung − *Department of Internal Medicine, Washington University School of Medicine, St. Louis, Missouri 63110, United States*; orcid.org/0000-0002-7189-9557

Scott L. Crick − *Auragent Bioscience, St. Louis, Missouri 63108, United States*

Complete contact information is available at: https://pubs.acs.org/10.1021/acsinfecdis.2c00086

Author Contributions

A.J.Q., S.L.C., C.W.F., and G.K.A. conceived this study. C.W., D.W.L., and G.K.A. developed SARS-CoV-2 N proteins. S.L.C., J.L., and M.M.Z. developed the microarrays and performed the experiments. M.M.Z. and A.J.Q. performed data analysis. C.W.F., M.L., and C.B. collected patient samples and clinical information. Initial manuscript draft was written by A.J.Q. with inputs and edits from all authors.

Funding

A.J.Q. was funded by the T32 Cancer Biology Award (NIH CA009547). Research was supported by Fast Grant #2161 (Emergent Ventures) to G.K.A., NIH grants (P01AI120943 and R01AI123926 to G.K.A., R01AI107056 to D.W.L., and R44AI155213 to S.L.C.). S.L.C., J.L., and M.M.Z. are shareholders of Auragent Bioscience. S.L.C. and M.M.Z. are currently employees of Auragent Bioscience.

Notes

The authors declare the following competing financial interest(s): S.L.C., J.L., and M.M.-U.Z. are shareholders of Auragent Bioscience. S.L.C. and M.M.-U.Z. are currently employees of Auragent Bioscience.

■ ABBREVIATIONS

AUC, area under the receiver−operator curve; *J*, Youden's index; LFA, lateral flow assay; LSPR, localized surface plasmon resonance; N FL, SARS-CoV-2 wild-type N protein; N NTD, SARS-CoV-2 N protein N-terminal domain; Orf3b, SARS-CoV-2 Orf3b protein; Orf8, SARS-CoV-2 Orf8 protein; PC, positive control; PF, plasmonic fluor; RFU, relative fluorescence units; ROC, receiver−operator characteristic; SEM, standard error of the mean; spike NTD, SARS-CoV-2 spike protein N-terminal domain; spike RBD, SARS-CoV-2 spike protein RNA-binding domain; spike S1, SARS-CoV-2 spike S1 domain protein; spike S2, SARS-CoV-2 spike S2 domain protein; SPRI, surface plasmon resonance imaging; BSA, bovine serum albumin; PBST, phosphate-buffered saline with Tween-20

■ REFERENCES

(1) Branson, B. M.; Owen, S. M.; Wesolowski, L. G.; Bennett, B.; Werner, B. G.; Wroblewski, K. E.; Pentella, M. A. *Laboratory Testing for the Diagnosis of HIV Infection: Updated Recommendations*; Centers for Disease Control and Prevention, 2014.

(2) Schillie, S.; Vellozzi, C.; Reingold, A.; Harris, A.; Haber, P.; Ward, J. W.; Nelson, N. P. Prevention of Hepatitis B Virus Infection in the United States: Recommendations of the Advisory Committee on Immunization Practices. *Morb. Mortal. Wkly. Rep. Recommendations and reports* **2018**, *67*, 1−31.

(3) Weinbaum, C. M.; Williams, I.; Mast, E. E.; Wang, S. A.; Finelli, L.; Wasley, A.; Neitzel, S. M.; Ward, J. W. Recommendations for identification and public health management of persons with chronic hepatitis B virus infection. *Morb. Mortal. Wkly. Rep. Recomm. Rep.* **2008**, *57*, 1−20.

(4) Lalwani, P.; Salgado, B. B.; Filho, I. V. P.; da Silva, D. S. S.; de Morais, T. B. d. N.; Jordão, M. F.; Barbosa, A. R. C.; Cordeiro, I. B.; Neto, J. N. d. S.; de Assunção, E. N.; Dos Santos, R. O.; Carvalho, N. O.; Sobrinho, W. B. S.; da Costa, C. F.; de Souza, P. E.; de Albuquerque, B. C.; Ganoza, C. A.; Araujo-Castillo, R. V.; Filho, S. A.; Lalwani, J. D. B. SARS-CoV-2 seroprevalence and associated factors in

Manaus, Brazil: baseline results from the DETECTCoV-19 cohort study. *Int. J. Infect. Dis.* **2021**, *110*, 141−150.
(5) Theel, E. S.; Harring, J.; Hilgart, H.; Granger, D.; McAdam, A. J. Performance Characteristics of Four High-Throughput Immunoassays for Detection of IgG Antibodies against SARS-CoV-2. *J. Clin. Microbiol.* **2020**, *58*, No. e01243-20.
(6) Haselmann, V.; Kittel, M.; Gerhards, C.; Thiaucourt, M.; Eichner, R.; Costina, V.; Neumaier, M. Comparison of test performance of commercial anti-SARS-CoV-2 immunoassays in serum and plasma samples. *Clin. Chim. Acta* **2020**, *510*, 73−78.
(7) Traugott, M.; Aberle, S. W.; Aberle, J. H.; Griebler, H.; Karolyi, M.; Pawelka, E.; Puchhammer-Stöckl, E.; Zoufaly, A.; Weseslindtner, L. Performance of severe acute respiratory syndrome coronavirus 2 antibody assays in different stages of infection: comparison of commercial enzyme-linked immunosorbent assays and rapid tests. *J. Infect. Dis.* **2020**, *222*, 362−366.
(8) Jääskeläinen, A.; Kuivanen, S.; Kekäläinen, E.; Ahava, M.; Loginov, R.; Kallio-Kokko, H.; Vapalahti, O.; Jarva, H.; Kurkela, S.; Lappalainen, M. Performance of six SARS-CoV-2 immunoassays in comparison with microneutralisation. *J. Clin. Virol.* **2020**, *129*, 104512.
(9) Farnsworth, C. W.; Anderson, N. W. SARS-CoV-2 Serology: Much Hype, Little Data. *Clin. Chem.* **2020**, *66*, 875−877.
(10) Muecksch, F.; Wise, H.; Batchelor, B.; Squires, M.; Semple, E.; Richardson, C.; McGuire, J.; Clearly, S.; Furrie, E.; Greig, N.; Hay, G.; Templeton, K.; Lorenzi, J. C. C.; Hatziioannou, T.; Jenks, S.; Bieniasz, P. D. Longitudinal Serological Analysis and Neutralizing Antibody Levels in Coronavirus Disease 2019 Convalescent Patients. *J. Infect. Dis.* **2020**, *223*, 389−398.
(11) Cheng, M. P.; Papenburg, J.; Desjardins, M.; Kanjilal, S.; Quach, C.; Libman, M.; Dittrich, S.; Yansouni, C. P. Diagnostic testing for severe acute respiratory syndrome−related coronavirus 2: a narrative review. *Ann. Intern. Med.* **2020**, *172*, 726−734.
(12) Hu, X.; An, T.; Situ, B.; Hu, Y.; Ou, Z.; Li, Q.; He, X.; Zhang, Y.; Tian, P.; Sun, D. Heat inactivation of serum interferes with the immunoanalysis of antibodies to SARS-CoV-2. *J. Clin. Lab. Anal.* **2020**, *34*, No. e23411.
(13) Tang, M. S.; Hock, K. G.; Logsdon, N. M.; Hayes, J. E.; Gronowski, A. M.; Anderson, N. W.; Farnsworth, C. W. Clinical Performance of the Roche SARS-CoV-2 Serologic Assay. *Clin. Chem.* **2020**, *66*, 1107−1109.
(14) Tang, M. S.; Hock, K. G.; Logsdon, N. M.; Hayes, J. E.; Gronowski, A. M.; Anderson, N. W.; Farnsworth, C. W. Clinical Performance of Two SARS-CoV-2 Serologic Assays. *Clin. Chem.* **2020**, *66*, 1055−1062.
(15) Bissonnette, L.; Bergeron, M. G. Diagnosing infections–current and anticipated technologies for point-of-care diagnostics and home-based testing. *Clin. Microbiol. Infect.* **2010**, *16*, 1044−1053.
(16) Bastos, M. L.; Tavaziva, G.; Abidi, S. K.; Campbell, J. R.; Haraoui, L.-P.; Johnston, J. C.; Lan, Z.; Law, S.; MacLean, E.; Trajman, A. Diagnostic accuracy of serological tests for covid-19: systematic review and meta-analysis. *BMJ [Br. Med. J.]* **2020**, *370*, 2516.
(17) Pallett, S. J. C.; Rayment, M.; Patel, A.; Fitzgerald-Smith, S. A. M.; Denny, S. J.; Charani, E.; Mai, A. L.; Gilmour, K. C.; Hatcher, J.; Scott, C.; Randell, P.; Mughal, N.; Jones, R.; Moore, L. S. P.; Davies, G. W. Point-of-care serological assays for delayed SARS-CoV-2 case identification among health-care workers in the UK: a prospective multicentre cohort study. *Lancet Respir. Med.* **2020**, *8*, 885−894.
(18) Pallett, S. J. C.; Rayment, M.; Patel, A.; Fitzgerald-Smith, S. A. M.; Denny, S. J.; Charani, E.; Mai, A. L.; Gilmour, K. C.; Hatcher, J.; Scott, C.; Randell, P.; Mughal, N.; Jones, R.; Moore, L. S. P.; Davies, G. W. Point-of-care serological assays for delayed SARS-CoV-2 case identification among health-care workers in the UK: a prospective multicentre cohort study. *Lancet Respir. Med.* **2020**, *8*, 885−894.
(19) Pickering, S.; Betancor, G.; Galão, R. P.; Merrick, B.; Signell, A. W.; Wilson, H. D.; Kia Ik, M. T.; Seow, J.; Graham, C.; Acors, S.; Kouphou, N.; Steel, K. J. A.; Hemmings, O.; Patel, A.; Nebbia, G.; Douthwaite, S.; O'Connell, L.; Luptak, J.; McCoy, L. E.; Brouwer, P.; van Gils, M. J.; Sanders, R. W.; Martinez Nunez, R.; Bisnauthsing, K.; O'Hara, G.; MacMahon, E.; Batra, R.; Malim, M. H.; Neil, S. J. D.; Doores, K. J.; Edgeworth, J. D. Comparative assessment of multiple COVID-19 serological technologies supports continued evaluation of point-of-care lateral flow assays in hospital and community healthcare settings. *PLoS Pathog.* **2020**, *16*, No. e1008817.
(20) Conklin, S. E.; Martin, K.; Manabe, Y. C.; Schmidt, H. A.; Miller, J.; Keruly, M.; Klock, E.; Kirby, C. S.; Baker, O. R.; Fernandez, R. E. Evaluation of serological SARS-CoV-2 lateral flow assays for rapid point-of-care testing. *J. Clin. Microbiol.* **2020**, *59*, No. e02020-20.
(21) Luan, J.; Seth, A.; Gupta, R.; Wang, Z.; Rathi, P.; Cao, S.; Gholami Derami, H.; Tang, R.; Xu, B.; Achilefu, S.; Morrissey, J. J.; Singamaneni, S. Ultrabright fluorescent nanoscale labels for the femtomolar detection of analytes with standard bioassays. *Nat. Biomed. Eng.* **2020**, *4*, 518−530.
(22) Wang, Z.; Luan, J.; Seth, A.; Liu, L.; You, M.; Gupta, P.; Rathi, P.; Wang, Y.; Cao, S.; Jiang, Q.; Zhang, X.; Gupta, R.; Zhou, Q.; Morrissey, J. J.; Scheller, E. L.; Rudra, J. S.; Singamaneni, S. Microneedle patch for the ultrasensitive quantification of protein biomarkers in interstitial fluid. *Nat. Biomed. Eng.* **2021**, *5*, 64−76.
(23) Kim, Y.; Wang, Z.; Li, C.; Kidd, K.; Wang, Y.; Johnson, B. G.; Kmoch, S.; Morrissey, J. J.; Bleyer, A. J.; Duffield, J. S.; Singamaneni, S.; Chen, Y. M. Ultrabright plasmonic fluor nanolabel-enabled detection of a urinary ER stress biomarker in autosomal dominant tubulointerstitial kidney disease. *Am. J. Physiol. Renal Physiol.* **2021**, *321*, F236−F244.
(24) Wang, Z.; Zhou, Q.; Seth, A.; Kolla, S.; Luan, J.; Jiang, Q.; Rathi, P.; Gupta, P.; Morrissey, J. J.; Naik, R. R.; Singamaneni, S. Plasmonically-enhanced competitive assay for ultrasensitive and multiplexed detection of small molecules. *Biosens. Bioelectron.* **2022**, *200*, 113918.
(25) Yung Hui, Y.; Lu, Y.-C.; Su, L.-J.; Fang, C.-Y.; Hsu, J.-H.; Chang, H.-C. Tip-enhanced sub-diffraction fluorescence imaging of nitrogen-vacancy centers in nanodiamonds. *Appl. Phys. Lett.* **2013**, *102*, 013102.
(26) Kemling, J. W.; Qavi, A. J.; Bailey, R. C.; Suslick, K. S. Nanostructured Substrates for Optical Sensing. *J. Phys. Chem. Lett.* **2011**, *2*, 2934−2944.
(27) Sagle, L. B.; Ruvuna, L. K.; Ruemmele, J. A.; Van Duyne, R. P. Advances in localized surface plasmon resonance spectroscopy biosensing. *Nanomedicine* **2011**, *6*, 1447−1462.
(28) Csáki, A.; Stranik, O.; Fritzsche, W. Localized surface plasmon resonance based biosensing. *Expert Rev. Mol. Diagn.* **2018**, *18*, 279−296.
(29) Langer, J.; Jimenez de Aberasturi, D.; Aizpurua, J.; Alvarez-Puebla, R. A.; Auguié, B.; Baumberg, J. J.; Bazan, G. C.; Bell, S. E. J.; Boisen, A.; Brolo, A. G.; Choo, J.; Cialla-May, D.; Deckert, V.; Fabris, L.; Faulds, K.; García de Abajo, F. J.; Goodacre, R.; Graham, D.; Haes, A. J.; Haynes, C. L.; Huck, C.; Itoh, T.; Käll, M.; Kneipp, J.; Kotov, N. A.; Kuang, H.; Le Ru, E. C.; Lee, H. K.; Li, J.-F.; Ling, X. Y.; Maier, S. A.; Mayerhöfer, T.; Moskovits, M.; Murakoshi, K.; Nam, J.-M.; Nie, S.; Ozaki, Y.; Pastoriza-Santos, I.; Perez-Juste, J.; Popp, J.; Pucci, A.; Reich, S.; Ren, B.; Schatz, G. C.; Shegai, T.; Schlücker, S.; Tay, L.-L.; Thomas, K. G.; Tian, Z.-Q.; Van Duyne, R. P.; Vo-Dinh, T.; Wang, Y.; Willets, K. A.; Xu, C.; Xu, H.; Xu, Y.; Yamamoto, Y. S.; Zhao, B.; Liz-Marzán, L. M. Present and Future of Surface-Enhanced Raman Scattering. *ACS Nano* **2020**, *14*, 28−117.
(30) Le Ru, E. C.; Etchegoin, P. G. Single-Molecule Surface-Enhanced Raman Spectroscopy. *Annu. Rev. Phys. Chem.* **2012**, *63*, 65−87.
(31) Pelton, M. Modified spontaneous emission in nanophotonic structures. *Nat. Photonics* **2015**, *9*, 427−435.
(32) Anger, P.; Bharadwaj, P.; Novotny, L. Enhancement and quenching of single-molecule fluorescence. *Phys. Rev. Lett.* **2006**, *96*, 113002.
(33) Vecchi, G.; Giannini, V.; Gómez Rivas, J. Shaping the fluorescent emission by lattice resonances in plasmonic crystals of nanoantennas. *Phys. Rev. Lett.* **2009**, *102*, 146807.

https://doi.org/10.1021/acsinfecdis.2c00086
ACS Infect. Dis. 2022, 8, 1468−1479

(34) Gerber, S.; Reil, F.; Hohenester, U.; Schlagenhaufen, T.; Krenn, J. R.; Leitner, A. Tailoring light emission properties of fluorophores by coupling to resonance-tuned metallic nanostructures. *Phys. Rev. B: Condens. Matter Mater. Phys.* **2007**, *75*, 073404.
(35) S. S. dos Santos, P.; M. M. M. de Almeida, J.; Pastoriza-Santos, I.; C. C. Coelho, L. Advances in Plasmonic Sensing at the NIR—A Review. *Sensors* **2021**, *21*, 2111.
(36) Hachim, A.; Kavian, N.; Cohen, C. A.; Chin, A. W. H.; Chu, D. K. W.; Mok, C. K. P.; Tsang, O. T. Y.; Yeung, Y. C.; Perera, R. A. P. M.; Poon, L. L. M.; Peiris, J. S. M.; Valkenburg, S. A. ORF8 and ORF3b antibodies are accurate serological markers of early and late SARS-CoV-2 infection. *Nat. Immunol.* **2020**, *21*, 1293−1301.
(37) Wu, C.; Qavi, A. J.; Hachim, A.; Kavian, N.; Cole, A. R.; Moyle, A. B.; Wagner, N. D.; Sweeney-Gibbons, J.; Rohrs, H. W.; Gross, M. L.; Peiris, J. S. M.; Basler, C. F.; Farnsworth, C. W.; Valkenburg, S. A.; Amarasinghe, G. K.; Leung, D. W. Characterization of SARS-CoV-2 nucleocapsid protein reveals multiple functional consequences of the C-terminal domain. *iScience* **2021**, *24*, 102681.
(38) Youden, W. J. Index for rating diagnostic tests. *Cancer* **1950**, *3*, 32−35.
(39) Qu, J.; Wu, C.; Li, X.; Zhang, G.; Jiang, Z.; Li, X.; Zhu, Q.; Liu, L. Profile of immunoglobulin G and IgM antibodies against severe acute respiratory syndrome coronavirus 2 (SARS-CoV-2). *Clin. Infect. Dis.* **2020**, *71*, 2255−2258.
(40) Padoan, A.; Sciacovelli, L.; Basso, D.; Negrini, D.; Zuin, S.; Cosma, C.; Faggian, D.; Matricardi, P.; Plebani, M. IgA-Ab response to spike glycoprotein of SARS-CoV-2 in patients with COVID-19: A longitudinal study. *Clin. Chim. Acta* **2020**, *507*, 164−166.
(41) Ma, H.; Zeng, W.; He, H.; Zhao, D.; Jiang, D.; Zhou, P.; Cheng, L.; Li, Y.; Ma, X.; Jin, T. Serum IgA, IgM, and IgG responses in COVID-19. *Cell. Mol. Immunol.* **2020**, *17*, 773−775.
(42) Hartman, A. L.; Nambulli, S.; McMillen, C. M.; White, A. G.; Tilston-Lunel, N. L.; Albe, J. R.; Cottle, E.; Dunn, M. D.; Frye, L. J.; Gilliland, T. H.; Olsen, E. L.; O'Malley, K. J.; Schwarz, M. M.; Tomko, J. A.; Walker, R. C.; Xia, M.; Hartman, M. S.; Klein, E.; Scanga, C. A.; Flynn, J. L.; Klimstra, W. B.; McElroy, A. K.; Reed, D. S.; Duprex, W. P. SARS-CoV-2 infection of African green monkeys results in mild respiratory disease discernible by PET/CT imaging and shedding of infectious virus from both respiratory and gastrointestinal tracts. *PLoS Pathog.* **2020**, *16*, No. e1008903.
(43) Sterlin, D.; Mathian, A.; Miyara, M.; Mohr, A.; Anna, F.; Claër, L.; Quentric, P.; Fadlallah, J.; Devilliers, H.; Ghillani, P.; Gunn, C.; Hockett, R.; Mudumba, S.; Guihot, A.; Luyt, C.-E.; Mayaux, J.; Beurton, A.; Fourati, S.; Bruel, T.; Schwartz, O.; Lacorte, J.-M.; Yssel, H.; Parizot, C.; Dorgham, K.; Charneau, P.; Amoura, Z.; Gorochov, G. IgA dominates the early neutralizing antibody response to SARS-CoV-2. *Sci. Transl. Med.* **2021**, *13*, No. eabd2223.
(44) Gorse, G. J.; Patel, G. B.; Vitale, J. N.; O'Connor, T. Z. Prevalence of Antibodies to Four Human Coronaviruses Is Lower in Nasal Secretions than in Serum. *Clin. Vaccine Immunol.* **2010**, *17*, 1875−1880.
(45) Prévost, J.; Gasser, R.; Beaudoin-Bussières, G.; Richard, J.; Duerr, R.; Laumaea, A.; Anand, S. P.; Goyette, G.; Benlarbi, M.; Ding, S.; Medjahed, H.; Lewin, A.; Perreault, J.; Tremblay, T.; Gendron-Lepage, G.; Gauthier, N.; Carrier, M.; Marcoux, D.; Piché, A.; Lavoie, M.; Benoit, A.; Loungnarath, V.; Brochu, G.; Haddad, E.; Stacey, H. D.; Miller, M. S.; Desforges, M.; Talbot, P. J.; Maule, G. T. G.; Cŏté, M.; Therrien, C.; Serhir, B.; Bazin, R.; Roger, M.; Finzi, A. Cross-Sectional Evaluation of Humoral Responses against SARS-CoV-2 Spike. *Cell Rep. Med.* **2020**, *1*, 100126.
(46) Ju, B.; Zhang, Q.; Ge, J.; Wang, R.; Sun, J.; Ge, X.; Yu, J.; Shan, S.; Zhou, B.; Song, S.; Tang, X.; Yu, J.; Lan, J.; Yuan, J.; Wang, H.; Zhao, J.; Zhang, S.; Wang, Y.; Shi, X.; Liu, L.; Zhao, J.; Wang, X.; Zhang, Z.; Zhang, L. Human neutralizing antibodies elicited by SARS-CoV-2 infection. *Nature* **2020**, *584*, 115−119.
(47) Anderson, E. M.; Goodwin, E. C.; Verma, A.; Arevalo, C. P.; Bolton, M. J.; Weirick, M. E.; Gouma, S.; McAllister, C. M.; Christensen, S. R.; Weaver, J.; Hicks, P.; Manzoni, T. B.; Oniyide, O.; Ramage, H.; Mathew, D.; Baxter, A. E.; Oldridge, D. A.; Greenplate, A. R.; Wu, J. E.; Alanio, C.; D'Andrea, K.; Kuthuru, O.; Dougherty, J.; Pattekar, A.; Kim, J.; Han, N.; Apostolidis, S. A.; Huang, A. C.; Vella, L. A.; Kuri-Cervantes, L.; Pampena, M. B.; Betts, M. R.; Wherry, E. J.; Meyer, N. J.; Cherry, S.; Bates, P.; Rader, D. J.; Hensley, S. E. Seasonal human coronavirus antibodies are boosted upon SARS-CoV-2 infection but not associated with protection. *Cell* **2021**, *184*, 1858−1864.
(48) Ng, K. W.; Faulkner, N.; Cornish, G. H.; Rosa, A.; Harvey, R.; Hussain, S.; Ulferts, R.; Earl, C.; Wrobel, A. G.; Benton, D. J.; Roustan, C.; Bolland, W.; Thompson, R.; Agua-Doce, A.; Hobson, P.; Heaney, J.; Rickman, H.; Paraskevopoulou, S.; Houlihan, C. F.; Thomson, K.; Sanchez, E.; Shin, G. Y.; Spyer, M. J.; Joshi, D.; O'Reilly, N.; Walker, P. A.; Kjaer, S.; Riddell, A.; Moore, C.; Jebson, B. R.; Wilkinson, M.; Marshall, L. R.; Rosser, E. C.; Radziszewska, A.; Peckham, H.; Ciurtin, C.; Wedderburn, L. R.; Beale, R.; Swanton, C.; Gandhi, S.; Stockinger, B.; McCauley, J.; Gamblin, S. J.; McCoy, L. E.; Cherepanov, P.; Nastouli, E.; Kassiotis, G. Preexisting and de novo humoral immunity to SARS-CoV-2 in humans. *Science* **2020**, *370*, 1339−1343.
(49) Post, N.; Eddy, D.; Huntley, C.; van Schalkwyk, M. C. I.; Shrotri, M.; Leeman, D.; Rigby, S.; Williams, S. V.; Bermingham, W. H.; Kellam, P.; Maher, J.; Shields, A. M.; Amirthalingam, G.; Peacock, S. J.; Ismail, S. A. Antibody response to SARS-CoV-2 infection in humans: A systematic review. *PLoS One* **2020**, *15*, No. e0244126.
(50) Patel, K.; Brown, S.; Dietzen, D. Listening closely when the volume is turned down: Challenges to small volume testing. *Clinical Laboratory News* May **2016**, *1*.
(51) Amanat, F.; Stadlbauer, D.; Strohmeier, S.; Nguyen, T. H. O.; Chromikova, V.; McMahon, M.; Jiang, K.; Arunkumar, G. A.; Jurczyszak, D.; Polanco, J.; Bermudez-Gonzalez, M.; Kleiner, G.; Aydillo, T.; Miorin, L.; Fierer, D. S.; Lugo, L. A.; Kojic, E. M.; Stoever, J.; Liu, S. T. H.; Cunningham-Rundles, C.; Felgner, P. L.; Moran, T.; García-Sastre, A.; Caplivski, D.; Cheng, A. C.; Kedzierska, K.; Vapalahti, O.; Hepojoki, J. M.; Simon, V.; Krammer, F. A serological assay to detect SARS-CoV-2 seroconversion in humans. *Nat. Med.* **2020**, *26*, 1033−1036.
(52) Freeman, J. D.; Rosman, L. M.; Ratcliff, J. D.; Strickland, P. T.; Graham, D. R.; Silbergeld, E. K. State of the science in dried blood spots. *Clin. Chem.* **2018**, *64*, 656−679.
(53) McDade, T. W.; Williams, S.; Snodgrass, J. J. What a drop can do: dried blood spots as a minimally invasive method for integrating biomarkers into population-based research. *Demography* **2007**, *44*, 899−925.
(54) Brinc, D.; Biondi, M. J.; Li, D.; Sun, H.; Capraru, C.; Smookler, D.; Zahoor, M. A.; Casey, J.; Kulasingam, V.; Feld, J. J. Evaluation of Dried Blood Spot Testing for SARS-CoV-2 Serology Using a Quantitative Commercial Assay. *Viruses* **2021**, *13*, 962.
(55) Gattinoni, L.; Chiumello, D. Anemia in the Intensive Care Unit: How Big Is the Problem? *Transfus. Altern. Transfus. Med.* **2002**, *4*, 118−120.
(56) Thavendiranathan, P.; Bagai, A.; Ebidia, A.; Detsky, A. S.; Choudhry, N. K. Do blood tests cause anemia in hospitalized patients? The effect of diagnostic phlebotomy on hemoglobin and hematocrit levels. *J. Gen. Intern. Med.* **2005**, *20*, 520−524.
(57) Chant, C.; Wilson, G.; Friedrich, J. O. Anemia, transfusion, and phlebotomy practices in critically ill patients with prolonged ICU length of stay: a cohort study. *Crit. Care* **2006**, *10*, R140.
(58) Mohn, K. G.-I.; Bredholt, G.; Zhou, F.; Madsen, A.; Onyango, T. B.; Fjelltveit, E. B.; Jalloh, S. L.; Brokstad, K. A.; Cantoni, D.; Mayora-Neto, M.; Temperton, N.; Langeland, N.; Cox, R. J. Durable T-cellular and humoral responses in SARS-CoV-2 hospitalized and community patients. *PLoS One* **2022**, *17*, No. e0261979.
(59) Klein, S. L.; Pekosz, A.; Park, H.-S.; Ursin, R. L.; Shapiro, J. R.; Benner, S. E.; Littlefield, K.; Kumar, S.; Naik, H. M.; Betenbaugh, M. J.; Shrestha, R.; Wu, A. A.; Hughes, R. M.; Burgess, I.; Caturegli, P.; Laeyendecker, O.; Quinn, T. C.; Sullivan, D.; Shoham, S.; Redd, A. D.; Bloch, E. M.; Casadevall, A.; Tobian, A. A. R. Sex, age, and hospitalization drive antibody responses in a COVID-19 convalescent plasma donor population. *J. Clin. Invest.* **2020**, *130*, 6141−6150.

https://doi.org/10.1021/acsinfecdis.2c00086
ACS Infect. Dis. 2022, 8, 1468−1479

(60) Wang, Z.; Morrissey, J. J.; Liu, L.; Wang, Y.; Zhou, Q.; Naik, R. R.; Singamaneni, S. Plasmonically Enhanced Ultrasensitive Epitope-Specific Serologic Assay for COVID-19. *Anal. Chem.* **2022**, *94*, 909−917.
(61) Barbara, A. M.; Loeb, M.; Dolovich, L.; Brazil, K.; Russell, M. Agreement between self-report and medical records on signs and symptoms of respiratory illness. *Prim. Care Respir. J.* **2012**, *21*, 145−152.
(62) Lynch, K. L.; Whitman, J. D.; Lacanienta, N. P.; Beckerdite, E. W.; Kastner, S. A.; Shy, B. R.; Goldgof, G. M.; Levine, A. G.; Bapat, S. P.; Stramer, S. L.; Esensten, J. H.; Hightower, A. W.; Bern, C.; Wu, A. H. B. Magnitude and Kinetics of Anti-Severe Acute Respiratory Syndrome Coronavirus 2 Antibody Responses and Their Relationship to Disease Severity. *Clin. Infect. Dis.* **2021**, *72*, 301−308.
(63) Ibarrondo, F. J.; Fulcher, J. A.; Goodman-Meza, D.; Elliott, J.; Hofmann, C.; Hausner, M. A.; Ferbas, K. G.; Tobin, N. H.; Aldrovandi, G. M.; Yang, O. O. Rapid Decay of Anti−SARS-CoV-2 Antibodies in Persons with Mild Covid-19. *N. Engl. J. Med.* **2020**, *383*, 1085−1087.
(64) Petersen, L. R.; Sami, S.; Vuong, N.; Pathela, P.; Weiss, D.; Morgenthau, B. M.; Henseler, R. A.; Daskalakis, D. C.; Atas, J.; Patel, A.; Lukacs, S.; Mackey, L.; Grohskopf, L. A.; Thornburg, N.; Akinbami, L. J. Lack of Antibodies to Severe Acute Respiratory Syndrome Coronavirus 2 (SARS-CoV-2) in a Large Cohort of Previously Infected Persons. *Clin. Infect. Dis.* **2020**, *73*, e3066−e3073.

https://doi.org/10.1021/acsinfecdis.2c00086
ACS Infect. Dis. 2022, 8, 1468−1479